Fuel 407 (2026) 137273

Contents lists available at ScienceDirect

Fuel

journal homepage: www.elsevier.com/locate/fuel

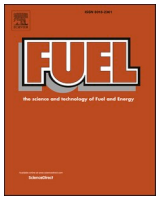

Full Length Article

In-situ growth of nanoaluminum in hydroxyl terminated polybutadiene and combustion characteristics

Ashvin Kumar Vasudevan [1], Erik Hagen [1], Yuxin Zhou, Keren Shi, Lei Yang, Michael R. Zachariah [*]

Departments of Chemical Engineering and Materials Science, University of California, Riverside, CA 92521, USA

ARTICLE INFO

Keywords:
Aluminum nanoparticles
Air-breathing combustion
Aluminum nanoparticle syntheses
Counterflow
Solid-fuel

ABSTRACT

The addition of aluminum nanoparticles (nAl) is attractive for solid fuels, due to their increased reactivity over their micron-sized counterparts. However, ejection of metal particles from the polymer surface during burning is difficult, resulting in sintering and eventual extinction of the reaction. It is speculated that part of this difficulty arises due to the inactive oxide shell, which insulates the active core of the nAl particle from potentially igniting. In this work, we present a method to synthesize nAl particles within hydroxyl-terminated polybutadiene (HTPB) through solvothermal synthesis. By doing this, the HTPB acts as a passivation layer and the particles distributed throughout the polymer do not contain an alumina shell. Synthesis experiments show that particle sizes can be varied from ~35–310 nm and loadings range from ~2.5–15 wt% aluminum. The results show that in-grown Al will enable propagation while added Al with a native oxide shell does not. The primary explanation on why in-grown Al is able to lift off the surface is that back diffusion of water and CO_2, which can react with the in-grown aluminum on the polymer surface, resulting in sufficient heat generation to heat and vaporize the surrounding polymer to lift the particles off the surface.

1. Introduction

Hydroxyl-terminated polybutadiene (HTPB) is a commonly used fuel component for solid propellant as well as the nascent fuel for air-breathing applications. The main benefits of using HTPB are its mechanical stability in a range of temperatures, ease of solid addition, as well as its applicability in rocket motors, hybrid systems and solid fuel ramjets [1]. Reactive metal particles such as aluminum offer the potential to improve the performance of the fuel without significantly compromising the mechanical properties of the polymer. While ammonium perchlorate based HTPB propellants have been widely studied [2], information about the performance of metal-based additives during HTPB combustion with air as the primary oxidation source is not as common. The specific impulse or of propellants has been shown to improve through addition of reactive metal powders such as aluminum, boron or magnesium [3].

Aluminum particles, mainly micron-sized aluminum, have been tested as a additives in HTPB due to their high density, stability and heat of oxidation [4]. Nano aluminum however, has not been extensively explored as an additive despite its faster ignition, quick and effective energy release and more complete combustion. One of the biggest impediments to using aluminum nanoparticles is that they tend to agglomerate and attach to the molten layer on the pyrolyzing surface when used with polymers such as HTPB [5]. Ultimately, this can inhibit regression by creating a barrier layer, preventing polymer pyrolysis products from efficiently leaving the surface. Molecular dynamics simulations show that the high interfacial forces between the oxide layer in aluminum nanoparticles and HTPB prevents it from being ejected by the lifting force generated by HTPB pyrolysis [6]. Quench studies of the heated HTPB composite showed agglomeration into clusters of up to 4 μm in size [7]. The smaller size and higher surface-to-volume ratios result in lower active aluminum content due to oxidation on the surface and thereby reduced energy released per unit volume [8]. Primary strategies to improve combustion of aluminum nanoparticles include coating with metals [9,10] or polymers/organic compounds [11,12] with the aim of improving energy release and reducing agglomeration. Thus, there remains a need for methods that both prevent sintering and provide uniform dispersion in polymers.

* Corresponding author.
E-mail address: mrz@engr.ucr.edu (M.R. Zachariah).
[1] These authors contributed equally.

https://doi.org/10.1016/j.fuel.2025.137273
Received 7 August 2025; Received in revised form 29 September 2025; Accepted 19 October 2025
Available online 29 October 2025

While there are top-down methods available to synthesize ultrafine aluminum, bottom-up approaches can provide better control over particle size and the passivating oxide layer. Aluminum hydride (AlH_3) is a suitable precursor for synthesizing aluminum nanoparticles of controllable size and lower size ranges by use of its amine complexes [13–15]. However, these methods can also produce agglomerated particles since the powder is formed as a precipitate. After synthesis, the particles cannot be dispersed effectively in the polymer. An in-situ approach as described in [16] can provide a uniform dispersion of aluminum nanoparticles formed in the polymer.

The primary application of this work is directed to fuels for air-breathing applications in which metallization is hoped to improve the volumetric energy density and combustion dynamics of the primary polymeric fuel. In this study, we explore the direct nucleation and growth of aluminum without an oxide layer directly within an HTPB matrix. The objective is to generate sufficient energy from an exothermic reaction between the aluminum particles and back-diffused CO_2 and H_2O at the pyrolysis zone to generate gas, and eject particles from the surface. The combustion characteristics are analyzed in a simple stagnation flow burner configuration. The size of the nucleated aluminum was controlled by various reaction conditions and the effect on combustion and regression was observed.

2. Experimental

2.1. Materials

An HTPB resin (R-45HTLO, RCS) was used for all experiments. A modified methylene diphenyl diisocyanate (MDI, RCS) and isodecyl pelargonate (IDP, RCS) served as curing agent and plasticizer respectively for HTPB. US Research Nanomaterials' aluminum nanopowder (99.9 %, 100 nm) was used to make nAl-HTPB composites.

N,N-dimethylethylamine alane complex (0.5 M in toluene) and titanium isopropoxide [$Ti(OCH(CH_3)_2)_4$] (97 %) were purchased from Sigma Aldrich. Tetrohydrofuran (99 %, Sigma) was used in selective experiments. These were used to synthesize nano-scale aluminum particles. More details can be found in Section 3.1.

2.2. Neat HTPB and physically mixed fuel grain preparation

Neat HTPB and nAl/HTPB (US Nano nAl) composite fuel grains were made by first mixing HTPB, MDI and IDP for 5 mins at 2000 RPM in a Thinky AR100 planetary mixer. Then, 5 wt% nAl was added and mixed for another 10 mins at 2000 RPM. The resulting paste was extruded into a 1 mL syringe (ID ~ 4.8 mm) and stored in a fume hood for 72 h to fully cure. A table with the details of the physically mixed fuel grains can be found in Table S1.

2.3. Transmission electron microscopy (TEM), and electron paramagnetic resonance (EPR)

A ThermoFisher Scientific Titan Themis 300 scanning transmission electron microscope was used to carry out TEM and STEM-EDS measurements of the aluminum nano powders synthesized under an accelerating voltage of 300 kV. A 300 mesh Lacey carbon grid with 63 μm holes was used in all measurements.

EPR measurements were carried out in a Bruker ESR5000 benchtop EPR with a 4 mm capillary tube over a range of 20–350 mT. Samples were loaded in a glovebox and sealed with a Fisherbrand Hemato-seal (tube sealant) for measurements. Four capillary tubes containing 50 μL of sample were analyzed for each run.

2.4. High-speed imaging, and three-color pyrometry

High-speed color imaging coupled with three-color pyrometry was carried out to investigate combustion events. Imaging was done with a Phantom Miro 110 camera and Nikon AF Micro Nikkor lens (aperture set at f/16, spatial resolution ~ 25 μm·pixel^{-1}). More details on the imaging can be found in previous publications [17–19]. Three-color imaging pyrometry was applied to the color-camera data to map surface temperatures as described elsewhere [17–19]. In short, color images were generated by debayering the raw Bayer pattern images. Temperatures were then estimated by taking ratios of the three-color channels (G/R, B/G and B/R) and comparing with theoretical temperatures assuming graybody emission. The cameras were calibrated with blackbody sources (ThorLabs SLS201L and Mikron M390) and have an expected uncertainty of ~200–300 K.

2.5. Digital inline holography (DIH)

Burning ejections were imaged by digital in-line holography (DIH) using a collimated, continuous-wave 532 nm laser (Coherent Verdi-V6), which was spatially filtered with a 5-μm pinhole and expanded to a 25-mm-diameter beam by 10 and 100 mm plano-convex lenses (Thorlabs model P5W, C060TMD-A, and LA1509-A). The in-line holograms were recorded on a high-speed CMOS camera (Phantom VEO 1310) at 10 kfps with 9 μs exposure time, using Infinity K2 Distamax long-distance microscope lenses (NTX tube with CF-4 objective) to achieve 2.8 μm/pixel over a 0.90 × 0.67 mm field of view. A band-pass filter (Thorlabs FLH532-4, 532 ± 2 nm) was mounted on the imaging optics to suppress combustion emissions, and the focal plane was positioned between the fuel rod and camera. A schematic of the DIH setup is shown in Fig. S6(a), and its operational principles detailed in previous studies [20–22]. This DIH setup enabled high-contrast diffraction patterns of >3 μm particles to be captured for three-dimensional tracking and particle sizing, after numerical reconstruction based on the Fresnel approximation [23].

2.6. Stagnation flow burner

Combustion evaluation of the composite grains was conducted using a stagnation flow burner, as shown in Fig. S6(b). The initial volumetric flow rate $\left(\dot{V}_0\right)$ of air is controlled by a mass flow controller (MKS model 1179, and 247D 4-channel readout). This air is flowed into a resistive heating tube (Omega 316 SS inline duct heater) with a thermocouple (type K) and a PID temperature controller (Inkbird) positioned before the exit. A series of six stainless steel mesh disks (McMaster, 40 × 40 then 100 × 100 mesh disks, model 9317 T552 and 9317 T555) were placed at the 19-mm-diameter nozzle exit to collimate the airflow, as shown in Fig. S6. The density of the heated air (ρ_{air}) scales with temperature according to the ideal gas law in Equation (1). Thus, the final air velocity (u_{air}) is computed from $\dot{V}_0$ with gas density correction and normalized by the area of the nozzle (A_{nozzle}) in Equation (2)

$$\rho_{air} = \frac{PM_{air}}{RT_{air}} \tag{1}$$

$$u_{air} = \frac{\dot{V}_0}{A_{nozzle}}\left(\frac{T_{air}}{T_0}\right) \tag{2}$$

where T_{air} is the temperature of the air read by the thermocouple and T_0 is the initial temperature of the air (~298 K).

On the fuel side, we used a 4.8-mm-diameter and 1-cm-length cylindrical grain. To maintain a constant 10 mm gap between the fuel surface and the oxidizer nozzle, we implemented a laser–photoresistor feedback loop driving a stepper motor (Thorlabs DRV225 with BSC201 controller) via an Arduino Uno microcontroller board and custom C# script. Prior to ignition, the stepper motor retracks, and a fuel grain is loaded into the burner. The laser is positioned ~2 mm above the top of the burner and aligned with the photoresistor. The motor then extrudes until the laser line is interrupted by the fuel grain, setting the initial height. During combustion, the signal from the photoresistor is tracked, and the fuel grain is extruded once the signal threshold is reached. After

each run, the recorded time and position data are fit to a linear curve, where the slope, or the extrusion rate of the stepper motor, gives the regression rate of the fuel grain. A schematic of the setup and sample burn rate data can be found in Fig. S6(b).

The strain rate, K (s^{-1}), quantifies the flux of gas to the surface of the fuel grain and is defined in Equation (3), where u_{air} is the velocity of the airflow, and d is the distance between the flow nozzle and the fuel surface. In this work, d was set to 10 mm to allow for imaging with the different cameras.

$$K = \frac{u_{air}}{d} \tag{3}$$

2.7. Kinetic and thermodynamic calculations

A one-dimensional counterflow diffusion flame model was implemented in Chemkin-Pro software [24] using USC Mech II [25] to estimate the diffusion flux of N_2, O_2, H_2O, and CO_2 and temperature distributions (at $K = 200\ s^{-1}$ and $T_{air} = 770\ K$). A multicomponent transport formulation is employed, with a boundary condition that specifies the experimental input mass flux rather than mass fraction, to allow back diffusion. Since the Chemkin model is for a pure-gas phase system, in order to model the solid fuel side, we assume that at the fuel boundary, HTPB → C_4H_6 gas [26–28]. The inlet temperature of C_4H_6 is assumed to be the same as the HTPB surface temperature measured with a IR camera, while the temperature of the inlet air is set to that measured by a K-type thermocouple within the air nozzle. The velocity of C_4H_6 is calculated based on the fuel regression rate, while the velocity of air is designated according to the MFC. The temperature of the flame at various heights above the molten HTPB surface (x) was measured by the rapid insertion of a B-type thin-wire thermocouple (OMEGA P30R-008) coupled with radiation heat loss correction [29,30].

3. Results and discussion

3.1. Synthesizing Al in HTPB, and curing mechanism

Our approach to avoid the combustion restrictions caused by the presence of the native oxide layer is to nucleate metal nanoparticles directly into the HTPB matrix before curing. In the case of aluminum, the most common method involves hydrogen abstraction from an alane precursor (usually N,N-dimethylethylamine alane) through a titanium catalyst [13,14]. To accomplish this within HTPB, a titanium-chelate complex is needed. The chelate acts as a nucleation center for aluminum while preventing polymer cross-linking [16]. We found that aluminum nanoparticles are formed in reaction with a uniform coating of HTPB resin before curing. The presence of the HTPB coating reduces agglomeration of aluminum particles [31] while also acting as a passivation agent. The HTPB resin was protected from AlH_3 attack by keeping the molar ratio of $Ti(OiPr)_4$:HTPB OH groups above 1:1. A diagram of this interaction can be seen in Fig. S2.

All experiments were carried out in a glovebox filled with argon at 1 atm. In general, 1–3 μL of $Ti(OiPr)_4$ was initially mixed with 2.5–5 mg of HTPB (~0.6 wt% of the total HTPB) to achieve a molar ratio range of Ti:HTPB of 2–10. The range of molar ratios was chosen to make sure there were minimal interactions of the HTPB terminal hydroxyl groups with AlH_3. This assumes that there are two terminal OH groups per HTPB monomer. Illustrations for interactions below this 1:1 limit can be seen in Fig. S3. Size control of the synthesized aluminum was brought about by varying the catalyst amounts. After mixing for ~15 min, 1.5–12 mL of alane was added and the resulting solution was stirred for 5 days on a stir plate at 40° C. A TEM image of the nucleated Al, along with EDS maps showing uniform coating of the HTPB on the synthesized Al particles can be seen in Fig. S7(a-d). This resulted in Al loadings of 2.5 – 20 wt%. The remaining HTPB (760 mg total) as well as the curing agent (MDI, 115 mg) and the plasticizer (IDP, 100 mg) were added and mixed in a Scientific Industries Vortex Genie 2 for 30 s to achieve consistent mixing. The resulting mixture was cured in a mold (ID ~ 0.48 mm) inside the glove box for three days. Details for different configurations and the resulting particle size range can be seen in Table S2.

In order to understand the complex reaction mechanism taking place, electron paramagnetic resonance (EPR) measurements were carried out during particle growth, and examined over the course of multiple days. Clarke et al. [13] showed in their synthesis of nascent Al (no polymer) that the formation of $Ti^{3+}(OiPr)_4$:AlH_3 clusters preceded aluminum nanocrystal formation and growth. EPR studies of reaction mixtures are shown in Fig. 1 and show the formation of $Ti^{3+}(OiPr)_4$-AlH_3 complexes at an Al:Ti molar ratio of 900:1. Testing showed that ~5 days were required for reaction completion, and safe curing without crosslinking of the HTPB. The EPR spectra contains three specific peaks at g-factors 2.07, 2.00 and 1.94. From Clarke et al. [13] the peak at 1.94 is expected to be the primary catalyst $Ti^{3+}(OiPr)_3$, and the peak at 2.00 is believed to be due to the formation of Ti-Al-H clusters. As seen in Fig. 1 (b), the catalyst's amount decreases over time with a corresponding increase in clusters formed. The Ti-Al-H clusters appear to get consumed after two days and only a weak peak is present after five days. The peak formed at 2.07 is likely the Al-Al clusters found in the alane precursor. A similar pattern is observed for the catalyst, where the Al-Al clusters are gradually consumed as the reaction proceeds to completion.

A proposed mechanism for nucleation of Al particles is shown in Fig. 2. This mechanism is similar in basic structure to the mechanism illustrated without a polymer in prior work [13]. Initial reaction of the alane complex forms a Ti-Al-H complex through hydrogen bridging. After H_2 abstraction, a $Ti(OiPr)_3$, which has higher activity than titanium isopropoxide, is formed. This initiates complex formation with neighboring alane, resulting in aluminum seeds formed close to the terminal hydroxyl groups of the HTPB. These seeds serve as a substrate for aluminum nanocrystal formation.

After two days of reaction, Fig. 1(b) shows that the presence of higher Ti-Al-H clusters with similar decreases in the catalyst and alane precursor when compared to the beginning of the reaction. The aluminum seeds shown in Fig. 2(5) are likely only formed after close to five days based on the EPR results. The slower reaction when compared to the experiments conducted in [13] is likely due to the drastically lower amounts of catalyst used for our study.

3.2. Synthesis limits, and size control

As previously mentioned, the ratios of Al:HTPB were dependent on the required loading of the aluminum in the final fuel grain while maintaining a Ti:HTPB ratio sufficient to prevent interaction of the hydroxyl terminal groups with the AlH_3 precursor; hence, precise control of constituents was necessary to ensure proper curing and control the size of the aluminum formed.

It was found that a molar ratio range of Ti:HTPB of 2–10 was necessary to ensure proper formation of the fuel grains. When the ratio was less than 2, the HTPB began to prematurely crosslink through the terminal hydroxyl groups. This resulted in a porous, brittle structure which could not be properly mixed with the remainder of the HTPB, MDI and IDP necessary to make a fuel grain. At a ratio greater than 10, viscous flakes formed and could not be properly mixed for later curing. Mechanisms for the formation of complexes for conditions with molar ratios 2–10 and <2 can be seen in Figs. S2 and S3 respectively. Size control of the aluminum nanoparticles was possible by changing the Ti catalyst amount. Within the molar ratio range, the size of the aluminum crystals formed decreased with increasing titanium catalyst amounts. The smallest particles were formed close to a molar ratio of 10. The different sizes obtained with changing Ti(OiPr)4 amounts are shown in Fig. 3. Particle size ranges were determined by taking the full-width half-max of a lognormal distribution fit. Size distributions can be seen in Fig. S1(a). Particles ranging from ~35–310 nm could be synthesized by changing the titanium catalyst amounts. As seen in Fig. 3, a smaller size

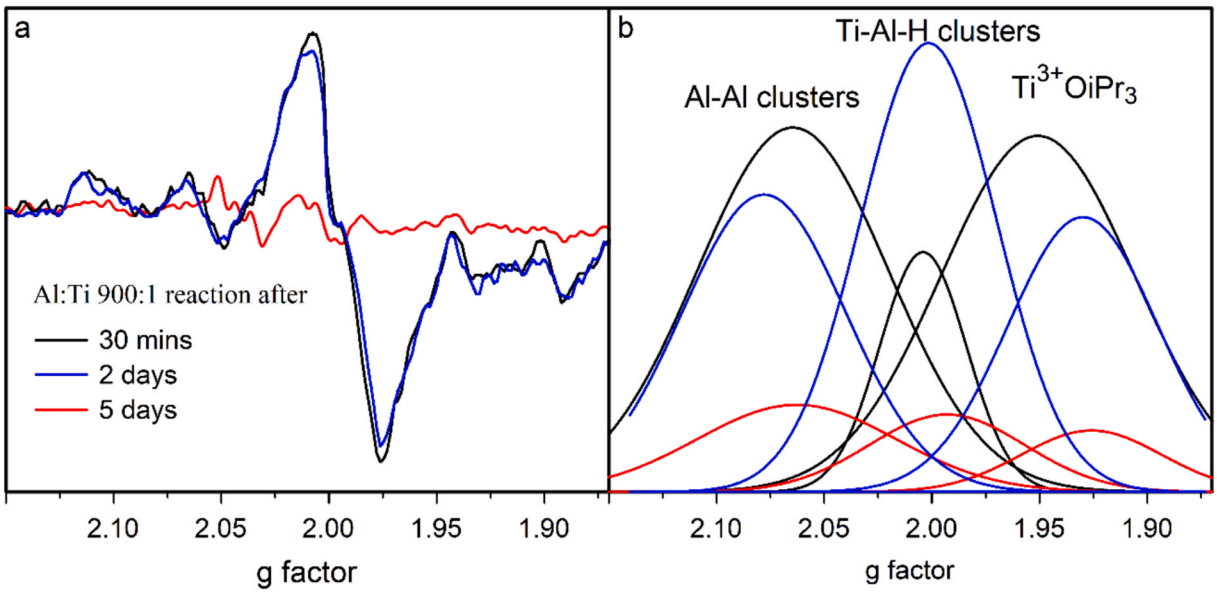

Fig. 1. (a) EPR spectra of the AlH_3:$Ti(OiPr)_4$:HTPB reaction mixtures. (b) Integrated EPR spectra after deconvolution.

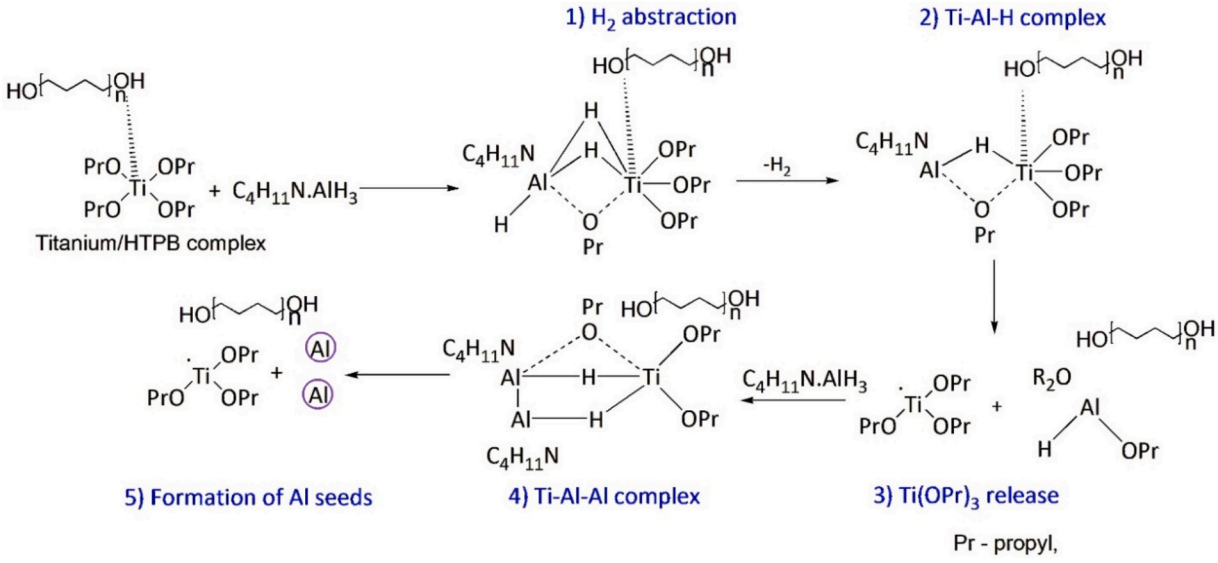

Fig. 2. Formation of Al seeds through Ti-Al-H complex formation and hydrogen abstraction.

ranges between ~5–35 nm could be synthesized; however, they formed viscous flakes upon the addition of curing agents, likely due to interactions with the $Ti(iPrO_4)$ catalyst, similar to interactions shown in [32].

Increases in aluminum precursor caused minor changes in the particle size distribution, as seen in Fig. S1(b). The condition with the molar ratio (Ti:HTPB) of 4:1 was used for these measurements. Small increases in the size ranges were observed with increased precursor amounts. Particle size was likely dependent on the number of initial aluminum seeds, which serve as nucleation sites. Increasing the amount of $Ti(OiPr)_4$ increased the number of nucleation sites, which in turn would lead to smaller particles at a constant Al loading. However, the increasing amounts of titanium catalyst required for synthesizing smaller size ranges resulted in increasingly porous samples on curing. Thermogravimetric analysis (TGA) of both the neat HTPB and the synthesized Al/HTPB composites shows minimal differences in decomposition after curing (Fig. S4).

3.3. Combustion of fuel grains in a stagnation flow burner

Fuel grain combustion was studied using an air stagnation flow burner, and imaged with a high-speed camera. Snapshots can be seen in Fig. 4. Physically mixed fuel grains consisted of HTPB and nAl/HTPB (5 wt%). Synthesized Al/HTPB composites had particle sizes ranging from 35-310 nm and loadings of 2.5–15 wt%. Tests were carried out at strain rates of 100–300 s^{-1} with an air temperature of 770 K. During combustion of the neat HTPB, the silhouette of the HTPB surface formed a hemispherical shape, with the flame forming a smooth dome, nearly parallel to the HTPB's surface (Fig. 4(a)). The added commercial nanoaluminum, nAl/HTPB, only propagated for approximately 2 mm, where upon bright aggregates appeared on the surface, eventually extinguishing the reaction (Fig. 4(b)).

All synthesized Al/HTPB fuel grains burned similarly. While HTPB had a smooth flame, the synthesized Al/HTPB fuel grains exhibited large bright bursts that frequently ejected from the flame (Fig. 4(c)). These ejections occluded the HTPB surface and made it difficult to identify the

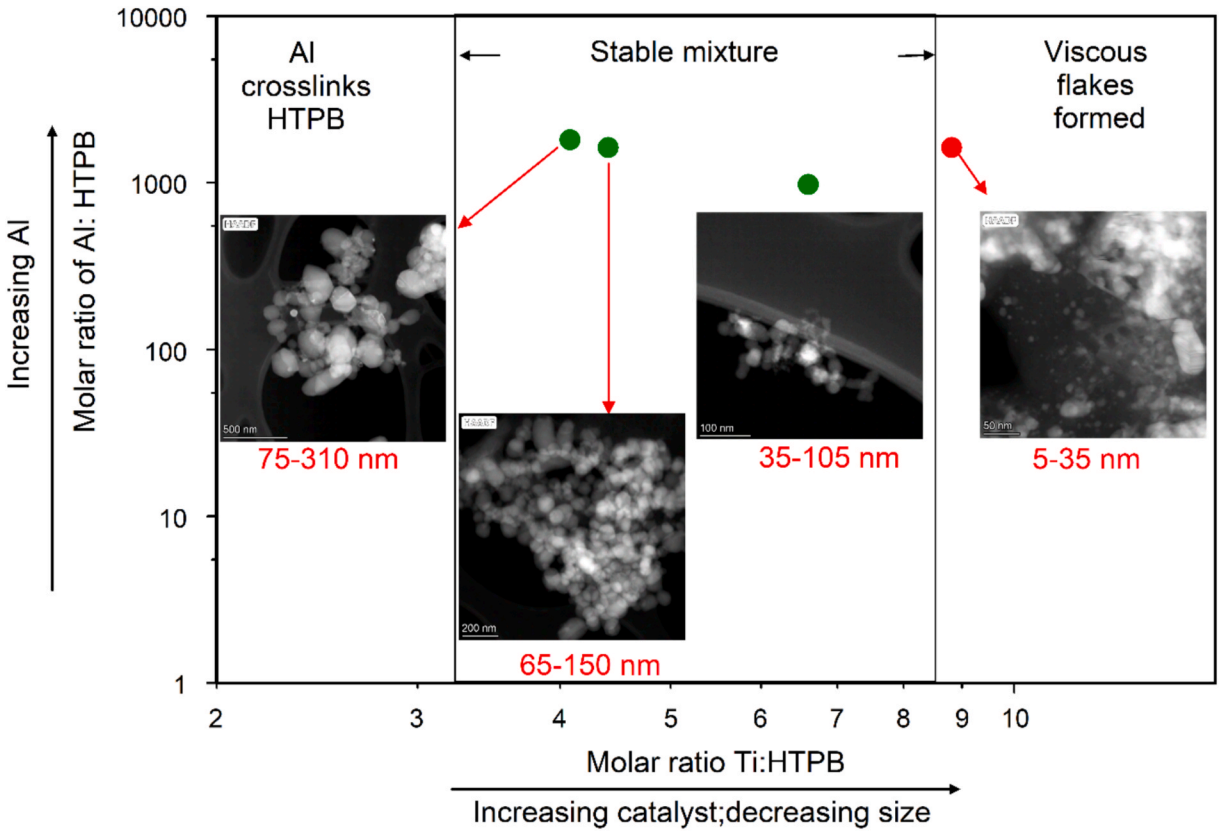

Fig. 3. Molar ratio limits of Al:HTPB and Ti:HTPB for which curing was achieved. NOTE: This accounts for HTPB used BEFORE the remaining HTPB is added for curing.

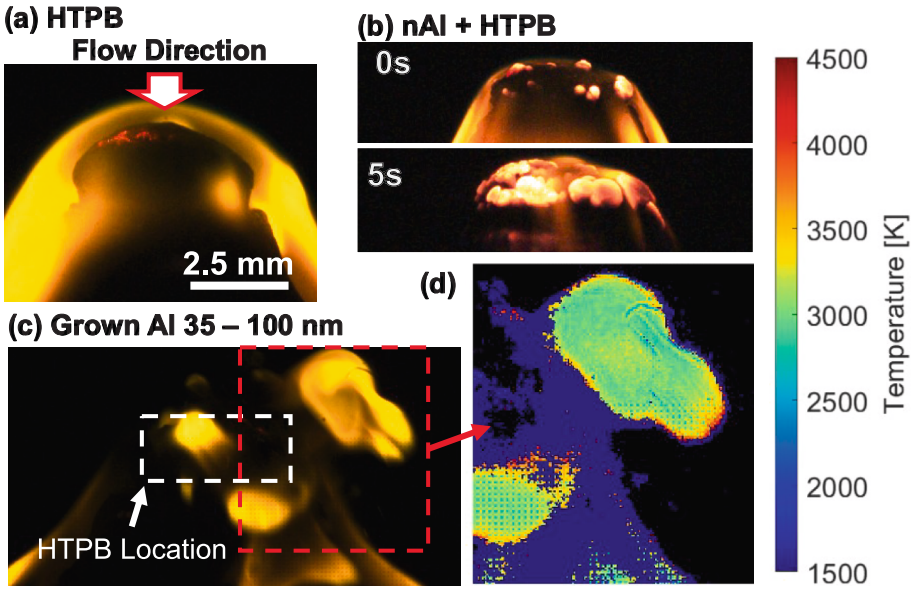

Fig. 4. High speed color camera images of (a) neat HTPB, (b) 5 wt% commercial nAl in HTPB and (c) 5 wt%, 35–100 nm nucleated Al. (d) shows a false color temperature map of the flame protrusions.

shape of the surface. Three-color pyrometry of these ejections shows that they are ~3000 K. Some streaks were observed; however, the bursts were the dominant feature of the flames. Neither of these features was observed in neat HTPB or in nAl/HTPB. These bursts were assumed to be caused by clouds of particles (shown in Fig. 4(d)) leaving the surface of the molten polymer. These disruptions to the flame were seen consistently for all aluminized samples of nucleated particles.

High magnification holograms were taken using a digital in-line holography (DIH) setup, allowing for visualization of the HTPB surface as it undergoes pyrolysis. Snapshots can be seen in Fig. S5. Most of what was seen was a cloud moving across the image field. We believe this cloud is a collection of the previously mentioned ejected nanoparticles.

3.4. Regression rates

Fig. 5(a) shows the regression rates of cured HTPB with 5 wt% additive of nucleated aluminum with different size distributions. As observed in Fig. 5(a), no clear effect of size is observed on the regression rate, although the number of particle ejections from the surface appears to increase for smaller-sized particles. Tests with increased nucleated aluminum (>5 wt%) could not be tested for all size ranges due to improper curing occurring likely due to titanium isoproxide-MDI interactions [32,33].

Fig. 5(b) shows the effect of Al mass loading on regression rate for HTPB samples with 50–100 nm grown aluminum. A maximum is found in the regression rates in all conditions at 10 wt% added aluminum with a marginal increase at this loading when compared to neat HTPB. Addition of aluminum beyond 15 wt% led to chunks of cured HTPB instead of one homogenous fuel grain. This is attributed to the high surface area of the nanoparticles. Similar results were seen when trying to physically mix HTPB with more than 15 wt% of 100 nm Al nanoparticles. As a result, no tests were carried out beyond a 15 wt% loading.

Adding up to 15 wt% aluminum did not show a noticeable increase in the regression rate of HTPB. One should keep in mind that in this diffusion flame configuration, the surface of the fuel is oxygen-starved, and it is the heat flux to the surface driving pyrolysis of HTPB. Thus, even though the added aluminum increases overall volumetric energy density, it does not necessarily increase regression rate. The key point is that the addition of nanoaluminum has shown to result in quenching, while in-situ grown Al enables continuous burning. This naturally leads to the question: why?

3.5. Combustion mechanism

In a prior study [6], it was found that nanosized Al particles have strong particle-polymer surface interactions i.e., the particle-HTPB binding energy was significantly higher than the kinetic energy imparted on the particles through pyrolysis; consequently, Al particles tend to sinter on the molten surface, progressively forming a passivation layer that inhibits further reaction, as illustrated in Fig. 7(a), as well as the aforementioned high-speed imaging results (Fig. 4).

To promote the ejection of Al particles, additional energy must be supplied to provide sufficient thrust. Fig. 6 presents the simulated distributions of key gas-phase species (H_2O, CO, CO_2, N_2, and O_2) and flame temperature in a counter-flow HTPB/air diffusion flame under conditions of strain rate $K = 200\ s^{-1}$ and air temperature $T_{air} = 770$ K, calculated by Chemkin-Pro [34] with USC Mech II [35].

O_2 concentration near the HTPB surface are too low to effectively generate exothermisity from reaction with Al to have any impact. However, H_2O and CO_2 may serve as alternative oxidizers. Notably,

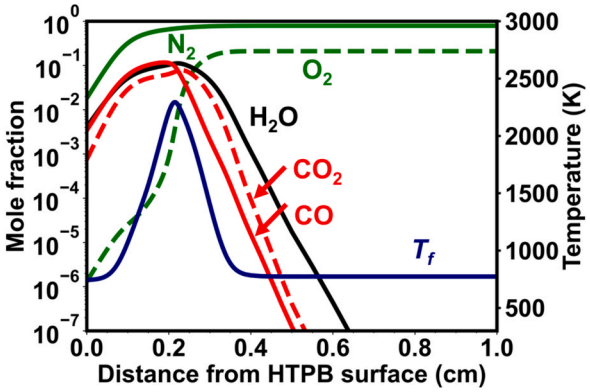

Fig. 6. Simulated profiles of the mol fractions of H_2O, CO, CO_2, N_2 and O_2 (left-y-axis) and temperature (right-y-axis).

Sarou-Kanian et al. [36] suggested that the oxidizing capability of CO_2 is enhanced with the presence of H_2O.

A rough estimation of the H_2O and CO_2 diffusion flux (J_{H_2O} and J_{CO_2}) can be made according to the gradient of H_2O and CO_2 in the narrow range of $x = 0$ to $x = 0.1$ cm, as shown by Eq. (4–8).

$$J_{H2O} = -D_{H_2O}\frac{dc_{H_2O}}{dx} = 0.085 mol/(m^2 s) \tag{4}$$

$$J_{CO2} = -D_{CO_2}\frac{dc_{CO_2}}{dx} = 0.030 mol/(m^2 s) \tag{5}$$

where D_{H_2O} and D_{CO_2} are the respective diffusion coefficients of H_2O and CO_2 calculated from the transport data in USC Mech II [35]. c_{H_2O} and c_{CO_2} are the molar concentrations of H_2O and CO_2.

Taking HTPB with 5 wt% Al addition as an example, the molar flux of Al J_{Al} can be calculated from the measured regression rate, as shown by Eq. (6).

$$J_{Al} = \frac{r\rho_{HTPB} w_{Al}}{M_{Al}} = 0.3\, mol/(m^2\, s) \tag{6}$$

where r is the measured regression rate; ρ_{HTPB} is the density of HTPB; w_{Al} is the weight percentage of Al and is; M_{Al} is the molar mass of Al.

Although the back-diffused H_2O and CO_2 are insufficient for the complete combustion of Al particles on the HTPB surface, they can partially oxidize Al. The heat release from the partial oxidation can be calculated by combining the standard enthalpy changes of Al- H_2O reaction ($\Delta H_1^0 = -487$ kJ/mol) and Al-CO_2 reaction ($\Delta H_2^0 = -553$ kJ/mol) with the molar ratios of Al to H_2O/CO_2, as follows.

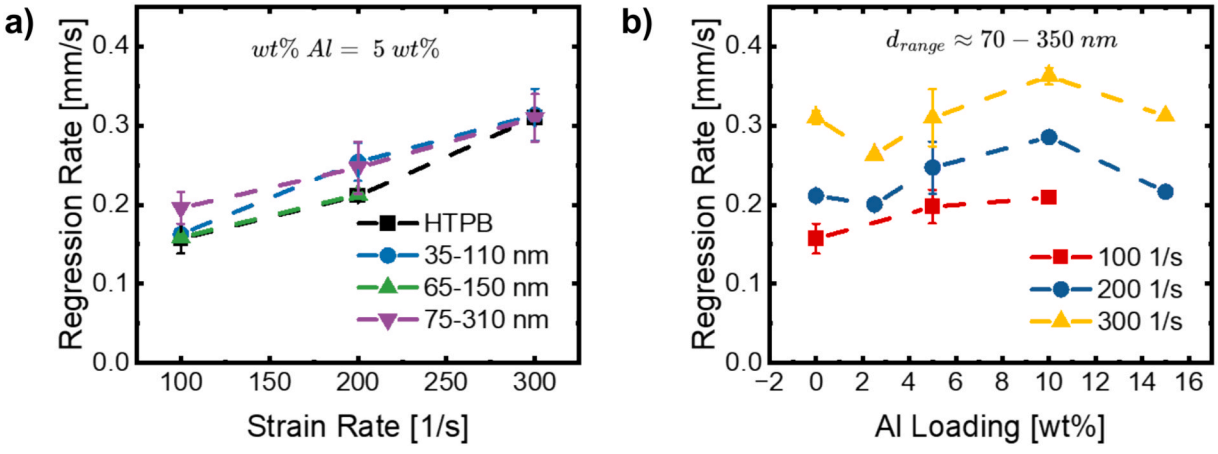

Fig. 5. Regression rates of fuel grains with a constant loading of 5 wt% Al, and different sizes (a) and a constant size range (90–350 nm) at various loadings of Al (b).

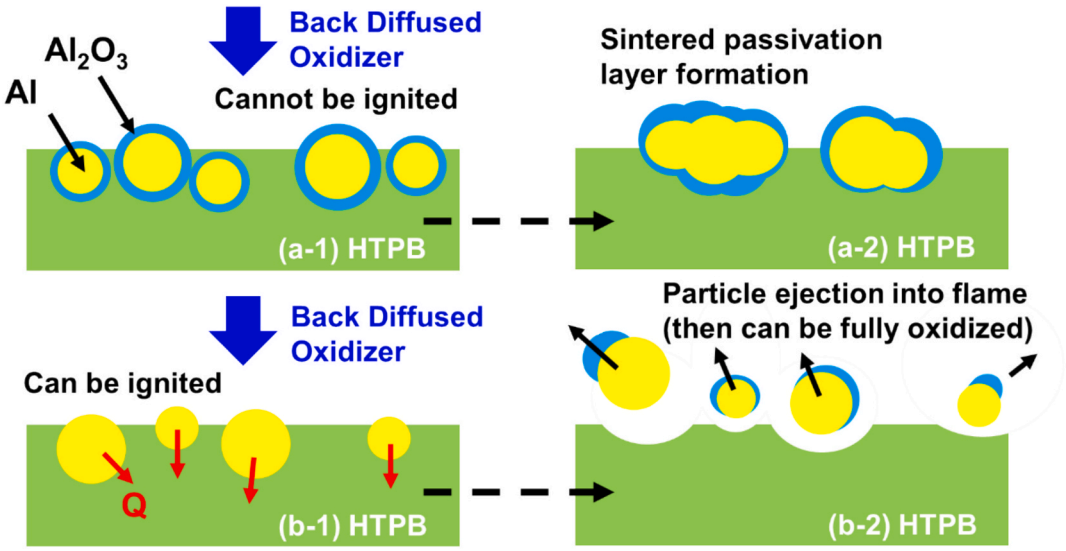

Fig. 7. Comparison between the behaviors of commercial Al nanoparticles (a) and grown Al nanoparticles (b) on the HTPB surface.

$$\Delta H_{oxidation} = \frac{J_{H_2O}}{1.5J_{Al}}\Delta H_1^0 + \frac{J_{CO_2}}{0.75J_{Al}}\Delta H_2^0 = -166kJ/mol \quad (7)$$

As for the pyrolysis of HTPB, previous experimental studies [28,37] show that HTPB has two decomposition stages, including an exothermic process without significant mass loss before 400 °C and an endothermic process with significant mass loss at ~450 °C. Considering the very thin layer (thickness ~ the diameter of Al particles) on the surface of HTPB, it should mainly undergo the endothermic process that releases gas-phase products. The enthalpy change in this process $E_{endo.HTPB}$ is roughly 0.1 kJ/g according to Chen et al. [28] Therefore, if the heat generated by the partial oxidation of Al particle with a volume of V_{Al} is all delivered to the surrounding HTPB, it can pyrolyze HTPB with a volume of V_{HTPB}. The relationship between V_{Al} and V_{HTPB} can be expressed by Eq. (8).

$$\frac{V_{HTPB}}{V_{Al}} = \frac{-\Delta H_{oxidation}\rho_{Al}}{M_{Al}E_{endo.HTPB}\rho_{HTPB}} = 10^2 \quad (8)$$

This demonstrates that once the Al particles are ignited on the HTPB surface, even if it is an incomplete oxidation, the heat generation can pyrolyze the surrounding HTPB and enhance regression rates.

4. Conclusion

In this work, we demonstrated that oxide-free nanosized aluminum particles were successfully grown and incorporated into an HTPB matrix. Unlike physically mixed commercial nAl, which sinters on the surface and quenches combustion, the in-grown particles remain reactive and enable sustained propagation. The Ti catalyst is shown to be the most significant factor for changing particle size as well as curing of the HTPB. Regression rate studies showed that there was no significant change from adding the Al particles, regardless of size and loading. High-speed color images showed that the flame structure of the aluminized composites was non-uniform and DIH suggests that these disturbances are caused by clouds of ejected nanoparticles. While there was no increase in regression rate, there was still an increase in the volumetric energy density of the composite. The primary distinction between in-grown and added aluminum appears to be the reaction between back diffused water and CO_2 with the particles on the HTPB surface. These species can react with the in-grown aluminum on the polymer surface, resulting in sufficient heat generation to heat the surrounding polymer to lift the particles off the surface. This approach provides a pathway toward designing energy-dense solid fuels for air-breathing propulsion systems.

CRediT authorship contribution statement

Ashvin Kumar Vasudevan: Writing – original draft, Methodology, Investigation. **Erik Hagen:** Writing – original draft, Investigation, Data curation. **Yuxin Zhou:** Writing – review & editing, Formal analysis, Data curation. **Keren Shi:** Writing – review & editing, Data curation. **Lei Yang:** Writing – review & editing, Visualization, Data curation. **Michael R. Zachariah:** Writing – review & editing, Supervision, Resources, Project administration, Methodology, Investigation, Funding acquisition, Conceptualization.

Declaration of competing interest

The authors declare that they have no known competing financial interests or personal relationships that could have appeared to influence the work reported in this paper.

Acknowledgments

This work was supported by the ONR.

Appendix A. Supplementary data

Supplementary data to this article can be found online at https://doi.org/10.1016/j.fuel.2025.137273.

Data availability

Data will be made available on request.

References

[1] Hedman TD. Radiation-induced pyrolysis of solid fuels for ramjet application. Propul Power Res 2016;5:87–96. https://doi.org/10.1016/j.jppr.2016.04.002.
[2] Chaturvedi S, Dave PN. Solid propellants: AP/HTPB composite propellants. Arab J Chem 2019;12:2061–8. https://doi.org/10.1016/j.arabjc.2014.12.033.
[3] Pang W, Li Y, DeLuca LT, Liang D, Qin Z, Liu X, et al. Effect of metal nanopowders on the performance of solid rocket propellants: a review. Nanomaterials 2021;11. https://doi.org/10.3390/nano11102749.
[4] Tian H, Niu X, Meng X, Jiang X, Gu X, Cai G. Numerical and experimental investigations of micro Al particle additive on the performances of HTPB hybrid rocket motors. Acta Astronaut 2024;220:449–61. https://doi.org/10.1016/j.actaastro.2024.04.045.
[5] Yuan J, Liu J, Zhou Y, Wang J, Xv T. Aluminum agglomeration of AP/HTPB composite propellant. Acta Astronaut 2019;156:14–22. https://doi.org/10.1016/j.actaastro.2018.11.009.

[6] Zhou Y, Zachariah MR. Computational Study on the lifting of aluminum particles from a hydroxyl-terminated polybutadiene burning surface. J Phys Chem C 2025; 129:5696–701. https://doi.org/10.1021/acs.jpcc.4c08542.
[7] Jayaraman K, Chakravarthy SR, Sarathi R. Quench collection of nano-aluminium agglomerates from combustion of sandwiches and propellants. Proc Combust Inst 2011;33:1941–7. https://doi.org/10.1016/j.proci.2010.06.047.
[8] Guo L, Song W, Hu M, Xie C, Chen X. Preparation and reactivity of aluminum nanopowders coated by hydroxyl-terminated polybutadiene (HTPB). Appl Surf Sci 2008;254:2413–7. https://doi.org/10.1016/j.apsusc.2007.09.043.
[9] Escot Bocanegra P, Chauveau C, Gökalp I. Experimental studies on the burning of coated and uncoated micro and nano-sized aluminium particles. Aerosp Sci Technol 2007;11:33–8. https://doi.org/10.1016/j.ast.2006.10.005.
[10] Ding X, Wang X, Zhu C, Hu J, Xu M, Ma M, et al. Research on ignition criterion and combustion behavior of aluminum alloy for lithium battery. Sci Rep 2025;15: 13734. https://doi.org/10.1038/s41598-025-97209-7.
[11] Lewis WK, Harruff BA, Gord JR, Rosenberger AT, Sexton TM, Guliants EA, et al. Chemical dynamics of aluminum nanoparticles in ammonium nitrate and ammonium perchlorate matrices: enhanced reactivity of organically capped aluminum. J Phys Chem C 2011;115:70–7. https://doi.org/10.1021/jp107264h.
[12] Sitompul HR, Budi RS, Restasari A, Abdillah LH, Ardianingsih R, Hartaya K, et al. Development of polyurethane-coated aluminum powder using solvent evaporation induced method. AIP Conf Proc 2022;2708:020001. https://doi.org/10.1063/5.0123148.
[13] Clark BD, DeSantis CJ, Wu G, Renard D, McClain MJ, Bursi L, et al. Ligand-dependent colloidal stability controls the growth of aluminum nanocrystals. J Am Chem Soc 2019;141:1716–24. https://doi.org/10.1021/jacs.8b12255.
[14] McClain MJ, Schlather AE, Ringe E, King NS, Liu L, Manjavacas A, et al. Aluminum nanocrystals. Nano Lett 2015;15:2751–5. https://doi.org/10.1021/acs.nanolett.5b00614.
[15] Yang S, Lu S, Li Y, Yu H, He L, Sun T, et al. Poly(ethylene oxide) mediated synthesis of sub-100-nm aluminum nanocrystals for deep ultraviolet plasmonic nanomaterials. CCS Chem 2020;2:516–26. doi: 10.31635/ccschem.020.202000141.
[16] Reid, Seal, Petersen. Compositions having aluminum particles dispersed in a continuous phase. U.S. 9,573,857 B2, n.d.
[17] Jacob RJ, Kline DJ, Zachariah MR. High speed 2-dimensional temperature measurements of nanothermite composites: probing thermal vs. Gas generation effects. J Appl Phys 2018;123:115902. https://doi.org/10.1063/1.5021890.
[18] Kline DJ, Rehwoldt MC, DeLisio JB, Barron SC, Wang H, Alibay Z, et al. In-operando thermophysical properties and kinetics measurements of Al-Zr-C composites. Combust Flame 2021;228:250–8. https://doi.org/10.1016/j.combustflame.2020.12.045.
[19] Kline DJ, Alibay Z, Rehwoldt MC, Idrogo-Lam A, Hamilton SG, Biswas P, et al. Experimental observation of the heat transfer mechanisms that drive propagation in additively manufactured energetic materials. Combust Flame 2020;215:417–24. https://doi.org/10.1016/j.combustflame.2020.01.020.
[20] Chen Y, Guildenbecher DR, Hoffmeister KNG, Cooper MA, Stauffacher HL, Oliver MS, et al. Study of aluminum particle combustion in solid propellant plumes using digital in-line holography and imaging pyrometry. Combust Flame 2017;182: 225–37. https://doi.org/10.1016/j.combustflame.2017.04.016.
[21] Huang J, Li S, Cai W, Qian Y, Berrocal E, Aldén M, et al. Quantification of the size, 3D location and velocity of burning iron particles in premixed methane flames using high-speed digital in-line holography. Combust Flame 2021;230:111430. https://doi.org/10.1016/j.combustflame.2021.111430.
[22] Mazumdar YC, Smyser ME, Heyborne JD, Slipchenko MN, Guildenbecher DR. Megahertz-rate shock-wave distortion cancellation via phase conjugate digital in-line holography. Nat Commun 2020;11:1129. https://doi.org/10.1038/s41467-020-14868-y.
[23] Schnars U, Falldorf C, Watson J, Jüptner W. Digital Holography. In: Schnars U, Falldorf C, Watson J, Jüptner W, editors. Digital holography and wavefront sensing: principles, techniques and applications, Berlin, Heidelberg: Springer Berlin Heidelberg; 2015, p. 39–68. doi: 10.1007/978-3-662-44693-5_3.
[24] ANSYS Chemkin-Pro n.d.
[25] USC Mech II n.d.
[26] Qian Y, Wang Z, Chen L, Liu P, Jia L, Dong B, et al. A study on the decomposition pathways of HTPB and HTPE pyrolysis by mass spectrometric analysis. J Anal Appl Pyrol 2023;170:105929. https://doi.org/10.1016/j.jaap.2023.105929.
[27] Tingfa D. Thermal decomposition studies of solid propellant binder HTPB. Thermochim Acta 1989;138:189–97. https://doi.org/10.1016/0040-6031(89)87255-7.
[28] Chen JK, Brill TB. Chemistry and kinetics of hydroxyl-terminated polybutadiene (HTPB) and diisocyanate-HTPB polymers during slow decomposition and combustion-like conditions. Combust Flame 1991;87:217–32. https://doi.org/10.1016/0010-2180(91)90109-O.
[29] Zhou Y, He Q, Sha Y, Shen C, You X. Effects of ferrocene addition on soot formation characteristics in laminar premixed burner-stabilized stagnation ethylene flames. J Aerosol Sci 2024;175:106265. https://doi.org/10.1016/j.jaerosci.2023.106265.
[30] Zhou Y, Shi K, Chowdhury M, Hagen E, Wang Y, Zachariah MR. Direct microscopic imaging of exploding aluminum/nitrocellulose mesoparticles to reveal the enhanced combustion mechanism. Fuel 2025;387:134348. https://doi.org/10.1016/j.fuel.2025.134348.
[31] Sossi A, Duranti E, Manzoni M, Paravan C, DeLuca LT, Vorozhtsov AB, et al. Combustion of HTPB-based solid fuels loaded with coated nanoaluminum. Combust Sci Technol 2013;185:17–36. https://doi.org/10.1080/00102202.2012.707261.
[32] Patten TE, Novak BM. "Living" titanium(IV) catalyzed coordination polymerizations of isocyanates. J Am Chem Soc 1991;113:5065–6. https://doi.org/10.1021/ja00013a055.
[33] Meth-Cohn O, Thorpe D, Twitchett HJ. Insertion reactions of titanium alkoxides with isocyanates and carbodiimides. J Chem Soc C 1970:132–5. https://doi.org/10.1039/J39700000132.
[34] ANSYS Chemkin Theory Manual 17.0 (15151) 2016.
[35] Wang H, You X, Joshi AV, Davis SG, Laskin A, Egolfopoulos F, et al. USC Mech Version II. High-temperature combustion reaction model of H2/CO/C1-C4 compounds 2007.
[36] Sarou-Kanian V, Rifflet JC, Millot F, Gökalp I. Aluminum combustion in wet and dry CO2: consequences for surface reactions. Combust Flame 2006;145:220–30. https://doi.org/10.1016/j.combustflame.2005.10.014.
[37] Lu Y-C, Kuo KK. Thermal decomposition study of hydroxyl-terminated polybutadiene (HTPB) solid fuel. Thermochim Acta 1996;275:181–91. https://doi.org/10.1016/0040-6031(95)02726-2.